ELSEVIER

Journal of Fluids and Structures 24 (2008) 977–993

JOURNAL OF FLUIDS AND STRUCTURES

www.elsevier.com/locate/jfs

Vortex-induced vibrations of a circular cylinder in laminar and turbulent flows

S. Pastò

Civil and Environmental Engineering Department, University of Florence, 3, v.S. Marta, 50139 Florence, Italy

Received 28 November 2006; accepted 5 January 2008
Available online 26 March 2008

Abstract

Experimental results on the behaviour of a freely vibrating circular cylinder in laminar and turbulent flows are presented. Wind tunnel tests have been performed by varying the cylinder roughness and the mass-damping parameter, $m^*\zeta$. The effects of surface roughness and flow turbulence have been considered in term of an effective Reynolds number, $\mathrm{Re}_{\mathrm{eff}}$. In this way, it has been possible to test the sample before and after the beginning of the cylinder boundary layer transition. It has been evidenced that $m^*\zeta$ is not the sole parameter influencing the response during lock-in; Reynolds number also plays an important role. If $m^*\zeta$ is fixed, the responses decrease as $\mathrm{Re}_{\mathrm{eff}}$ increases. Moreover, it has been observed that the cylinder may experience vortex-induced vibrations even in the critical $\mathrm{Re}_{\mathrm{eff}}$ regime characterized by a cessation of coherent vortex shedding in steady configuration. The effects of $m^*\zeta$ and $\mathrm{Re}_{\mathrm{eff}}$ on the critical velocity (the velocity at which the maximum amplitude of response is approached), on the wideness of the lock-in range, and on the wake correlation length are also discussed.

Keywords: Lock-in; Vortex-induced vibrations; Across-wind oscillations; Vortex capture; Vortex shedding

1. Introduction

A clear insight into the mechanism of vortex shedding has been proposed by Gerrard (1966). Gerrard has postulated that a vortex continues to grow until is strong enough to draw the opposite shear layer across the near wake. The oppositely signed vorticity cuts off further supply of circulation to the growing vortex, which is then shed, flowing downstream.

Such vortices have a shedding frequency, f_{vs}, following the well-known law, $\mathrm{St} = f_{vs}D/U$, where St is the Strouhal number depending on the Reynolds number, Re, U is the flow velocity, D is the across-wind dimension of the body.

The vortex shedding is very affected by Reynolds number. An extensive review of the analysis of vortex shedding past steady circular cylinders is given by Williamson (1996). The major Reynolds regimes of vortex shedding are reported in Lienhard (1966). In particular, at $\mathrm{Re} = 5$ the flow does not detach from the cylinder surface, so the fluid follows the cylinder contours. In the range $5 \leqslant \mathrm{Re} \leqslant 45$, the flow separates from the back of the cylinder and the near wake is characterized by a symmetric pair of vortices. If Re is further increased, the wake becomes unstable and the vortices shed alternately from the cylinder sides. The wake is given by two vortices of opposite sign (vortex street) and is

E-mail address: stefanop@dicea.unifi.it

0889-9746/$ - see front matter
doi:10.1016/j.jfluidstructs.2008.01.001

laminar. In the range $150 \leqslant \mathrm{Re} \leqslant 300$ the wake becomes turbulent, although the boundary layer on the cylinder remains laminar. In the *subcritical* range ($300 < \mathrm{Re} \leqslant 1.5 \times 10^5$) the vortex shedding is strong and periodic, while in the range $1.5 \times 10^5 < \mathrm{Re} \leqslant 3.5 \times 10^6$ the cylinder boundary layer becomes turbulent, and the average drag coefficient decreases. In this range, named *transitional* regime, the spectra of the shedding frequencies broaden and the regular vortex shedding starts to be compromised until it disappears completely in the *critical* subrange $3 \times 10^5 < \mathrm{Re} \leqslant 3.5 \times 10^6$. In the *supercritical* regime, $\mathrm{Re} > 3.5 \times 10^6$, coherent vortex shedding is established again. In this regime the boundary layer of the cylinder surface is turbulent, the turbulent flow separation point moves forward so that the wake widens and the drag coefficient increases.

The mechanism of vortex shedding is also affected by the flow turbulence. Rounded bodies, immersed in turbulent flow, experience a transition of the boundary layer over the body surface. The main consequence is the anticipation of the *transitional* Reynolds regime. In particular, the boundary layer transition Reynolds number decreases and the fall in the drag coefficient experienced by the cylinder is anticipated as well. However, the characterization of the turbulent effects should take into account both the intensity of turbulence, I_u, and the longitudinal length scale, L_u. Basu (1986) observed that in the subcritical regime, with $L_u/D \approx 1$, the drag decreases first until $I_u = 4\%$ and then it increases as I_u grows. This behaviour has been ascribed to the circumstance that low turbulence intensities tend to break the coherence of the vortex shedding, while high levels induce earlier transition of the shear layers. According to Surry (1969) small scale turbulence ($L_u/D = 0.36$) is better able to anticipate transition than large scale turbulence ($L_u/D = 4.3$). Blackburn and Melbourne (1996) underlined that high turbulence intensities (up to 18%) with small scale ($L_u/D = 0.5$) increase the *postcritical* lift force. In this circumstance, the Strouhal number has been noticed to increase, $\mathrm{St} = 0.23$.

From the foregoing one may deduce that varying both I_u and L_u it is not possible to distinguish the effect of each individual parameter. Vickery (1990) suggested that the combined effect of I_u and L_u may be considered by means of the parameter $T_a = I_u(L_u)^{-1/3}$. ESDU (1980) considers this parameter in the definition of the effective Reynolds number, $\mathrm{Re}_{\mathrm{eff}}$, which allows the assessment of the Reynolds regime induced by the flow turbulence.

Another parameter influencing the vortex shedding mechanism is the surface roughness of the cylinder. As reported by Scruton and Rogers (1971), increasing the cylinder roughness the transitional Reynolds regime and the fall in the drag coefficient are anticipated.

If the cylinder may vibrate in the across-wind direction, and the vortex shedding frequency, f_{vs}, and natural frequency of the body, f_o, approach a common value, lock-in occurs triggering a complex fluid–structure interaction which extends along a certain velocity range and results in a change of the dynamics of the body and of its unsteady wake.

A body performing vortex-induced vibrations (VIVs) is a deformable suspended body, with reduced mass $m^* = \rho_m/\rho_f$ (where ρ_m and ρ_f are the body and fluid mass density, respectively) and structural damping ζ, oscillating in the across-wind direction as a consequence of an aeroelastic interaction with its unsteady wake along which the two shear layers interact each other bounding the same wake.

Increasing the flow velocity, U, within the lock-in interval, the spacing between the shear layers surrounding the body increases initially providing a virtual increase of the body diameter. This justifies the introduction of the added mass coefficient, $C_a = \Delta m/\rho_f V_b$ (V_b is the body volume), whose value is sensitively different from its value in inviscid flow whenever the vorticity is not confined by a tiny superficial shear layer [see e.g. Basset, 1888; Sarpkaya, 1977, 2000]. The existence of the added mass makes the body vibrate within the lock-in interval at a frequency of oscillation equal but even lower or greater than its natural frequency.

The lock-in range is controlled mainly by the reduced mass m^*, whereas the maximum response amplitude is driven by the product $m^*\zeta$ (Khalak and Williamson, 1999). The mass-damping parameter, $m^*\zeta$, derived from different studies and it is englobed in the definition of further parameters used to plot the influence of $m^*\zeta$ on the maximum response amplitude. The most well known are the Scruton number, $\mathrm{Sc} = \pi^2(m^*\zeta)$, and the Skop–Griffin number (Skop, 1974), $\mathrm{SG} = 2\pi^3 S_t^2(m^*\zeta)$. The higher is the mass-damping parameter the lower is the response [see e.g. Feng, 1968; Sarpkaya, 2004; Williamson and Govardhan, 2004].

By now, it is well known that a body performing VIVs induces a substantial increase in the wake correlation [see e.g. Toebes, 1969; Novak and Tanaka, 1975; Ramberg and Griffin, 1976] and in the drag coefficient [see e.g. Bishop and Hassan, 1964; Tanida et al., 1973; Sarpkaya, 1978], changes the wake dynamics [see e.g. Williamson and Roshko, 1988; Zdravkovich, 1997], and determines a decrease of the vortex formation length (Zdravkovich, 1997) so increasing the vortical force and the base suction (Griffin and Ramberg, 1975).

Zdravkovich (1982) observed that a phase shift, between the lift force and the cylinder displacement, occurred at the velocity at which the cylinder attained its maximum response. Williamson and Roshko (1988) ascribed this phase shift to a change in vortex structure, from the so called 2S mode to the 2P mode, which outlines at least two response branches, the initial branch and the lower branches. Khalak and Williamson (1999) showed the existence of the upper branch at lower $m^*\zeta$. Nevertheless, Klamo et al. (2006) found that $m^*\zeta$ is not the sole parameter influencing the response

branches. In particular, they found that low damping and sufficiently high Re provide three branches (initial, upper and lower) and large response amplitudes, whereas high damping or low Re furnish two branches (initial and lower) and small response amplitude. An extensive discussion on the influence of Re on the response amplitude is also given by Govardhan and Williamson (2006).

The branch transition may be hysteretic [see e.g. Feng, 1968; Khalak and Williamson, 1999; Govardhan and Williamson, 2000; Williamson and Govardhan, 2004; Singh and Mittal, 2005]. In particular, Williamson and Govardhan (2004) pointed out in their review paper that hysteresis might occur at low Re. Singh and Mittal (2005) confirmed this and discovered hysteresis at the upper Re range of synchronization as well. Klamo et al. (2006) found an hysteretic behaviour even in the transition from the lower branch to the desynchronization region, at low Re.

Humphries and Walker (1988) performed VIV tests on a circular cylinder in the range $5 \times 10^4 \leqslant \mathrm{Re} \leqslant 4 \times 10^5$. They observed a substantial increase of the drag coefficient even in the critical Reynolds regime where it drops usually in the case of steady cylinder.

In the present work, an elastically mounted circular cylinder has been tested in the CRIACIV boundary layer wind tunnel. The investigation has been performed with different mechanical and flow configurations. In particular, smooth and rough cylinders with four damping levels have been studied both in laminar and turbulent flows. The results have been discussed to highlight the main features of the lock-in phenomenon varying the system damping and the Reynolds regimes. In particular, the experimental campaign has focused on the evaluation of the influence of the mass-damping parameter and of the Reynolds number on the response amplitude, on the wideness of the synchronization range, and on the wake correlation. Finally, some issues concerning the phase between the lift force and the cylinder motion have been stated by discussing the results obtained by means of the model of Bearman (1965).

2. Experimental procedures

VIVs tests on a circular cylinder have been performed in the CRIACIV laboratory.[1] The wind tunnel has a cross-section 2.2 m wide and 1.6 m high, slightly divergent from the inlet to the test-section whose dimensions are 2.4 m × 1.6 m. The global length of the wind tunnel, from the inlet to the end of the diffusers, is about 24 m. The values of the velocities are obtained by means of both the regulation of the pitch of the ten blades constituting the fan, and the rotating speed. The maximum velocity attainable is 35 m/s.

2.1. The sample tested

The sample tested in the wind tunnel is a circular hollow cylinder 2.3 m long and with a diameter of about 0.155 m. The cylinder is composed of three parts connected together through a pre-compression bar (Fig. 1(a)). Each part is made of two carbon-fibre surfaces connected to each other by a honeycomb material in a way such that the overall thickness is of about 5 mm. The whole cylinder is stiff enough to limitate the elastic deflection of the cylinder. In this way the hypothesis of elastically suspended rigid body is guaranteed.

The sample has been placed transversally as regards the wind direction in the middle height of the test-section, 0.80 m from the wind tunnel floor and ceiling (Figs. 1(a)–(c)), and it has been elastically suspended outside the wind tunnel by means of eight springs (four for each side) connected to the cylinder axes. Such axes jut out of the slits of the wind tunnel sides (Figs. 1(a) and (c)). The springs have been connected to two external frames fixed to the wind tunnel.

The longitudinal displacement has been restrained by means of four prestressed cables (each one 5 m long) placed upstream and downstream starting from each cylinder extremity.

Two additional devices, providing damping to the system, have been placed at the extremities of the cylinder (Figs. 1(a) and (c)). Damping has been assured by a bar pushing in a water tank. Additional rods, placed at the end of each bar, have been used to obtain three different damping levels. So, the total number of damping levels has been 4, the model self-damping included. Each damping level has been determined by means of decay tests in still air. The results are reported in Table 1.

Three anemometers have been placed in the wake of the cylinder (Figs. 1(a) and (b)), 3 diameters downstream and 2 diameters downside from the cylinder axis, in order to get f_{vs} and the correlation of the wake vortices. The anemometers have been positioned, respectively, at $L/2, L/3, L/6$ (L is the cylinder length) from the middle of the cylinder (Fig. 1(a)).

The transversal displacement of the model undergoing VIVs has been logged by means of laser transducers (Figs. 1(a) and (c)) monitoring the motion of the cylinder extremities with no contact.

[1]Inter-University Research Center of Building Aerodynamics and Wind Engineering.

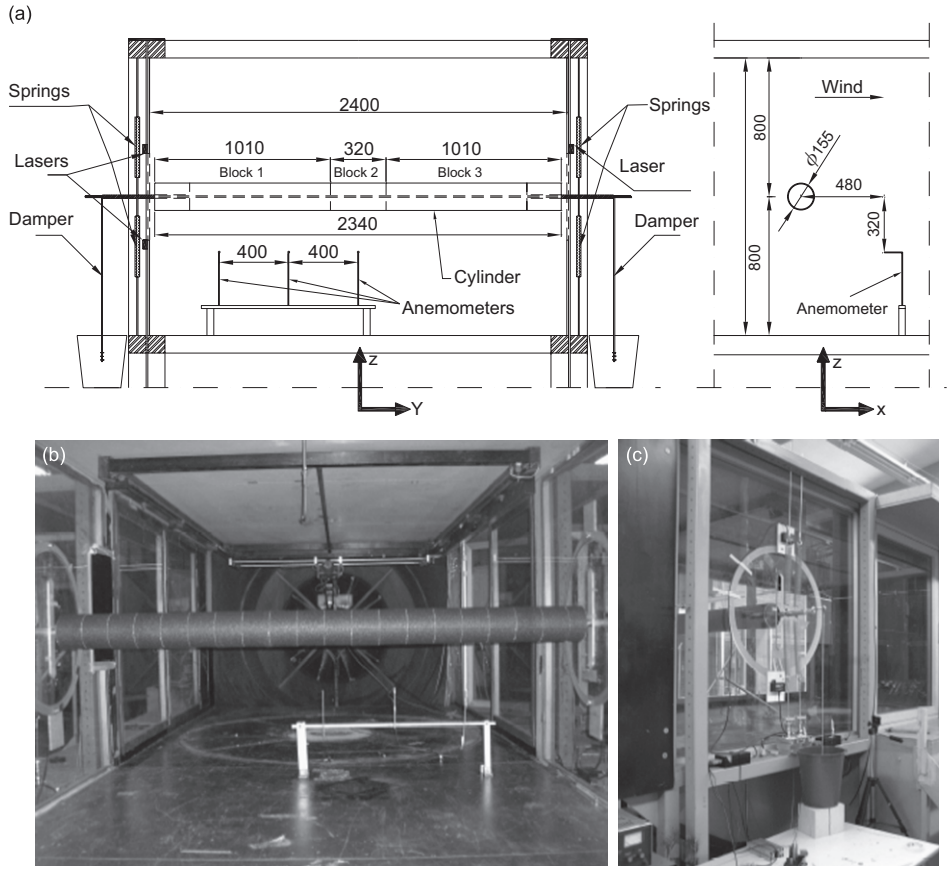

Fig. 1. Cylinder set-up in the CRIACIV wind tunnel.

Table 1
Mechanical properties of the cylinder in two different configurations

		Units	Configurations	
			I	II
D		m	0.155	0.155
L		m	2.3	2.3
k_s/D		–	0	0.003
k		N/m	5840	5840
m		kg	7.155	8.341
m^*		–	133.75	155.83
f_o		Hz	4.547	4.211
ζ	Structural	–	0.0024	0.0024
ζ	1 Rod	–	0.0039	0.0039
ζ	2 Rods	–	0.0046	0.0046
ζ	3 Rods	–	0.0050	0.0050

D: cylinder diameter; L: cylinder length; k_s: roughness thickness; k: system stiffness; m: system mass; m^*: reduced mass; ζ: system damping ratio; f_o: natural frequency of oscillation.

2.2. Mechanical characteristics of the sample

The cylinder has been tested in two configurations differing from each other for the superficial roughness. In particular, an emery cloth with a mean thickness of 0.5 mm ($k_s = 0.5$ mm) has been used together with the high turbulence in order to vary the Re regime in which the cylinder performed VIVs. The mechanical properties of the cylinder are reported in Table 1, whereas each experimental run is identified by the nomenclature of Table 3.

2.3. Characteristics of the flow

Two turbulence levels have been generated by two grids with different meshes [for further details see Pastò (2005)], placed at about 4.5 m upstream from the cylinder. A procedure has been performed in order to get the turbulence intensity, I_u, and length scale, L_u, in the test-section (see Table 2). In particular, the model has been removed from the test-section and replaced by an hot-wire probe placed in the middle height of the test-section, 0.80 m far from its floor, and able to log the frequency contents of the longitudinal component of the incoming flow. The spectra obtained over a wide range of flow velocities, the same utilized during dynamical tests, have been then fitted by the von Karman spectrum (von Karman, 1948) which reads

$$\frac{fS_{uu}(f)}{\tilde{u}^2} = \frac{4fL_u/U}{[1 + 70.8(fL_u/U)^2]^{5/6}}, \tag{1}$$

where $S_{uu}(f)$ is the spectrum of the longitudinal component of the wind velocity, and f is the generic frequency. By fitting the experimental data with the von Karman spectrum in Eq. (1), it has been possible to draw out L_u for each velocity (Figs. 2(a) and (b)). In the same range of flow velocities, the intensity of turbulence, I_u, has been computed by means of the well-known formula $I_u = \tilde{u}/U$, where U and $\tilde{u}$ are, respectively, the mean and the standard deviation of the longitudinal component of the flow velocity. Finally, the average value of L_u and I_u have been calculated (see Table 2).

2.4. Strouhal number, St

For a generic body, changes of St correspond to changes in the aerodynamic behaviour. By maintaining constant the mean flow velocity, different body sections may display different St according to their shape and the flow acceleration about it: for instance, a square-section cylinder presents St lower than a circular cylinder [see e.g. Blevins, 1990].

Considerable differences also occur in the aerodynamic performance of a body for very small changes of the same St. This variation is strongly dependent on Re regimes so that, for a circular cylinder in the critical regime, St is undefined since vortex shedding does not occur. Moreover, St depends on the surface roughness, k_s (or on the roughness ratio, k_s/D), I_u and L_u [see e.g. ESDU, 1996; Schewe, 2001].

A set of experimental tests have been performed to get the Strouhal numbers of the smooth and rough steady cylinders in laminar and turbulent flows. The results of the experimental investigation of St are reported in Figs. 3(a) and (b), and in Table 2.

It has been possible to obtain the Strouhal frequencies, and hence St, only in two flow conditions: laminar flow and low turbulence flows. This restriction appears because the surface roughness and the higher turbulence level induce an early transition of the shear layer near the cylinder surface. In particular, the operating Re regime seems to move to the *critical* one where the vortex shedding past steady cylinder disappears completely preventing the assessment of St.

In order to validate the assumption of a shift towards the *critical* regime, Re has been evaluated by means of the numerical approach proposed by ESDU (1980) and described in the following section.

Table 2
The characteristics of the flows considered during lock-in tests, and of the respective cylinder Strouhal numbers

Flow	I_u (%)	L_u (m)	St
Laminar	–	–	0.2074
Low turbulence	3.0	0.044	0.2095
High turbulence	13.5	0.160	–

I_u: turbulence intensity; L_u: length scale; St: Strouhal number.

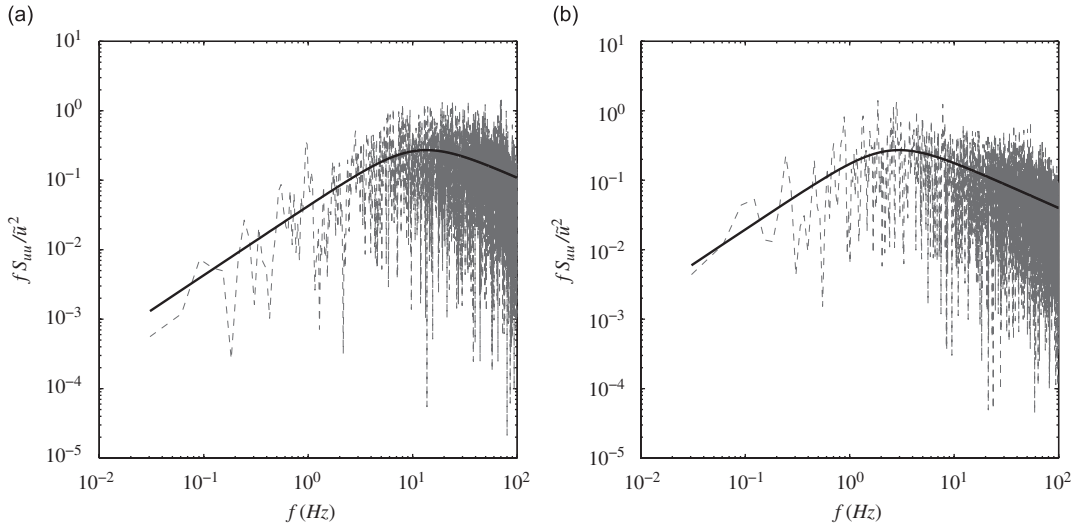

Fig. 2. Spectra of the fluctuating component of the longitudinal flow velocity. (a) Smaller mesh grid: $I_u = 3\%$, $L_u = 0.044\,\mathrm{m}$ and (b) larger mesh grid: $I_u = 13.5\%$, $L_u = 0.160\,\mathrm{m}$. —, fitted von Karman spectrum; -.-, logged spectrum.

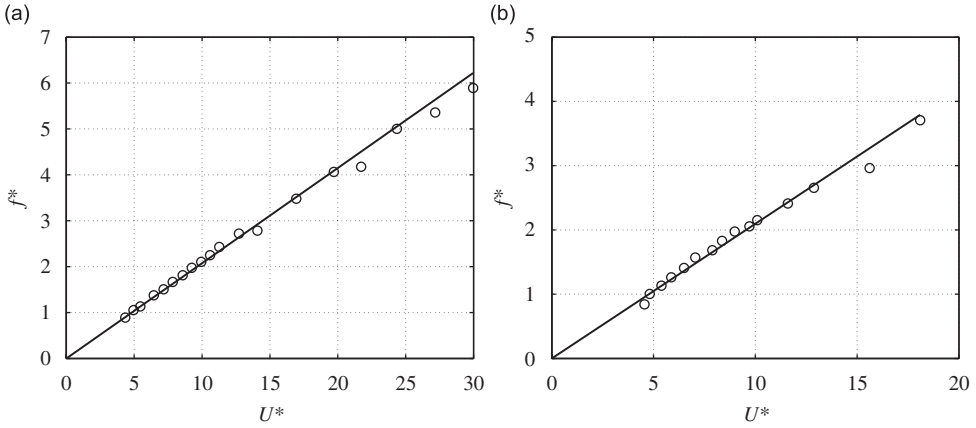

Fig. 3. Experimental investigation to determine St of the steady cylinder. The plots show the variation of the frequency ratio $f^* = f_{vs}/f_o$ with the reduced velocity $U^* = U/(f_o D)$. (a) Strouhal number law for the smooth cylinder in laminar flow: $\mathrm{St} = 0.2074$ $(3.153 \times 10^4 \leqslant \mathrm{Re} \leqslant 2.176 \times 10^5)$ and (b) Strouhal number law for the smooth cylinder in low turbulence flow: $\mathrm{St} = 0.2095$ $(3.321 \times 10^4 \leqslant \mathrm{Re} \leqslant 1.320 \times 10^5)$. ○, Experimental data; —, fitted data.

3. Reynolds regimes

As remarked in the Introduction, the vortex shedding process depends strongly on Re, turbulence characteristics of the approaching flow, and surface roughness.

According to ESDU (1980), for a stationary cylinder, it is possible to signify the combined effects of Re, flow turbulence and surface roughness in terms of an effective Reynolds number, $\mathrm{Re}_{\mathrm{eff}}$. In particular, $\mathrm{Re}_{\mathrm{eff}}$ is written analytically as follows:

$$\mathrm{Re}_{\mathrm{eff}} = \lambda_T \lambda_R \mathrm{Re}, \tag{2}$$

where λ_T and λ_R are coefficients taking, respectively, into account the turbulence characteristics of the flow and the cylinder surface roughness.

The explicit procedure to determine λ_T and λ_R is not reported here for the sake of brevity, but it is fully described in ESDU (1980). The ranges of $\mathrm{Re}_{\mathrm{eff}}$ have been computed for each set of turbulence and cylinder surface roughness. As

Table 3
Identifiers and characteristics of the vortex-induced-vibration runs

Run	Configuration	$m^*\zeta$	Flow	$Re\|_{at\ lock\text{-}in}[10^5]$	$Re_{eff}\|_{at\ lock\text{-}in}[10^5]$	Re_{eff} regime	$Re_{eff}\|_{A^*_{max}}[10^5]$
a_1	I	0.321	Laminar	0.340–0.499	0.340–0.499	Subcritical	0.426
a_2	I	0.522	Laminar	0.320–0.436	0.320–0.436	Subcritical	0.379
a_3	I	0.615	Laminar	0.312–0.383	0.312–0.383	Subcritical	0.373
a_4	I	0.669	Laminar	0.312–0.358	0.312–0.358	Subcritical	0.358
b_1	I	0.321	Low turbulence	0.330–0.478	2.076–3.055	Transitional	2.76
b_2	I	0.522	Low turbulence	0.312–0.404	1.910–2.630	Transitional	2.39
b_3	I	0.615	Low turbulence	0.320–0.382	1.991–2.475	Transitional	2.34
b_4	I	0.669	Low turbulence	0.312–0.366	1.913–2.362	Transitional	2.30
c_1	I	0.321	High turbulence	0.320–0.448	3.760–4.612	Critical	4.14
c_2	I	0.522	High turbulence	0.321–0.384	3.789–4.227	Critical	4.00
c_3	I	0.615	High turbulence	0.308–0.390	3.689–4.270	Critical	3.98
c_4	I	0.669	High turbulence	0.307–0.373	3.679–4.154	Critical	3.96
d_1	II	0.374	High turbulence	0.279–0.379	3.456–4.197	Critical	4.76
d_2	II	0.608	High turbulence	0.288–0.346	3.530–3.970	Critical	4.68
d_3	II	0.717	High turbulence	0.274–0.347	3.405–3.980	Critical	4.67
d_4	II	0.780	High turbulence	0.277–0.343	3.434–3.954	Critical	4.67

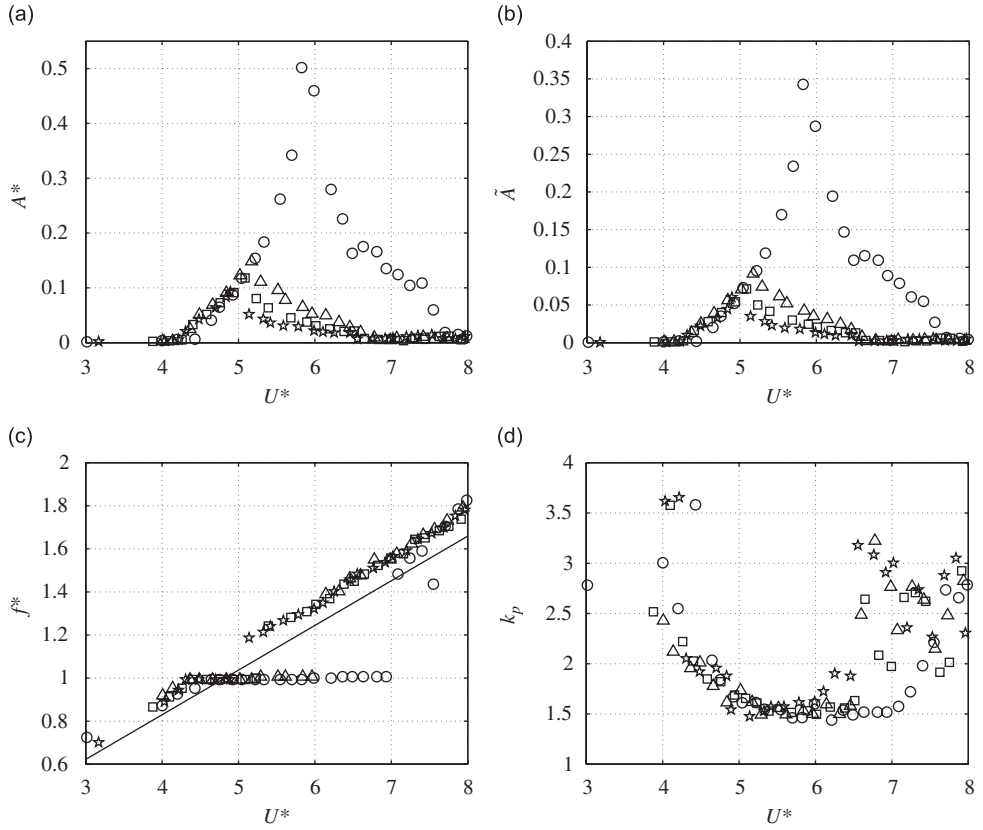

Fig. 4. Variation with U^* of the dimensionless amplitude, (a) A^*, of the standard deviation of the dimensionless amplitude, (b) $\widetilde{A}$, of the frequency ratio (c) f^*, and of the peak factor, (d) k_p: ○, Run a_1; △, Run a_2; □, Run a_3; ☆, Run a_4. Solid line in graph (c): Strouhal frequencies for the steady cylinder, St = 0.2074.

reported in the Introduction, the regimes of vortex shedding depend on Re ranges. The results of the procedure have been compared with those Re ranges and they are reported in Table 3. Such results validate the assumption of a shift towards the *critical* regime for both the smooth and the rough cylinders immersed in the high turbulence flow.

Clearly, direct measurements of the Re regimes may be suitable. However, ESDU (1980) provides qualified data based on the major researches on the subject. The drag coefficients obtained experimentally by Buresti and Launaro (1980) on a rough cylinder are in good agreement with those of ESDU (1970) and Achenbach (1971). Moreover, the sectional pressure distributions of a circular cylinder in the subcritical regime measured by Buresti and Martini (1980) are in good agreement with those proposed by ESDU (1970).

4. Vortex-induced-vibration tests

VIV tests have been performed on the smooth and the rough cylinders by using four damping levels, in laminar and turbulent flows. The summary and the identifiers of the tests have been reported in Table 3.

The research purposes have dealt with the evaluation of (i) the synchronization range in terms of the ratio between the vortex shedding frequency and the body natural frequency; (ii) the effects of the synchronization in terms of the cylinder response and the wake correlation; (iii) the influence of the damping on the response, on the wideness of the synchronization range, and on the wake correlation; (iv) the effects of low and high turbulence on the synchronization.

The tests have been carried out in progressive regime: the velocity of air has been increased at small increments while the cylinder was oscillating at its steady-state amplitude. The same tests have been repeated by decreasing velocities. Nevertheless, since no hysteretic behaviour has been encountered during dynamical tests (Pastò, 2005), only the results obtained by increasing velocities are reported here.

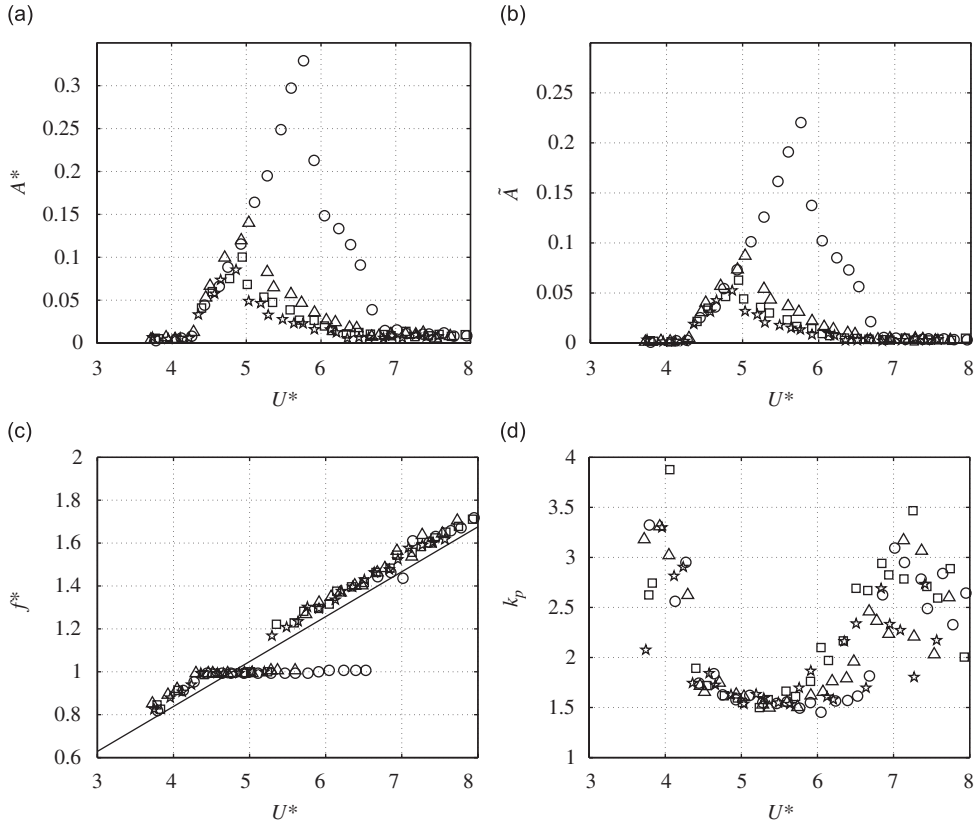

Fig. 5. Variation with U^* of the dimensionless amplitude, (a) A^*, of the standard deviation of the dimensionless amplitude, (b) $\tilde{A}$, of the frequency ratio, (c) f^*, and of the peak factor, (d) k_p: ○, Run b_1; △, Run b_2; □, Run b_3; ☆, Run b_4. Solid line in graph (c): Strouhal frequencies for the steady cylinder, St = 0.2095.

The dimensionless response is given by $A^* = \hat{y}/D$ and $\widetilde{A} = \tilde{y}/D$, where $\hat{y}$ and $\tilde{y}$ are, respectively, the maximum and the standard deviation of the steady-state amplitude of the response time history $y = y(t)$, and D is the cylinder diameter. The peak factor is computed by means of $k_p = \hat{y}/\tilde{y}$, since the mean value of the response, $\bar{y}$, is practically null.

The range of lock-in may be evaluated by the graphs showing the trend of $f^* = f_{vs}/f_o$ versus the reduced velocity $U^* = U/Df_o$.

Moreover, the wake correlation function has been computed by means of the data logged by the three anemometers placed in the near wake (see Section 2.1). By integrating the correlation function along the wake, it has been possible to obtain the correlation length, L_c, that is the length along which the near wake, and hence its action on the body, is almost fully correlated:

$$L_c = \int_0^L r(\Delta z)\,\mathrm{d}\Delta z. \tag{3}$$

The normalized wake correlation function, $r(\Delta z)$, is given as a function of the distance Δz, with z referring to the spanwise coordinate:

$$r(\Delta z) = \frac{\overline{u_w(z,t)u_w(z+\Delta z,t)}}{\widetilde{u}_w(z)\widetilde{u}_w(z+\Delta z)}, \tag{4}$$

where the overbar denotes a time average, u_w is the longitudinal component of the wake flow velocity, and $\widetilde{u}_w$ is its standard deviation. In order to compute L_c in Eq. (3), $r(\Delta z)$ has been fitted, along the spanwise coordinate, with an exponential function given by $r(\Delta z) = \exp(-c\Delta z)$, where c is a constant.

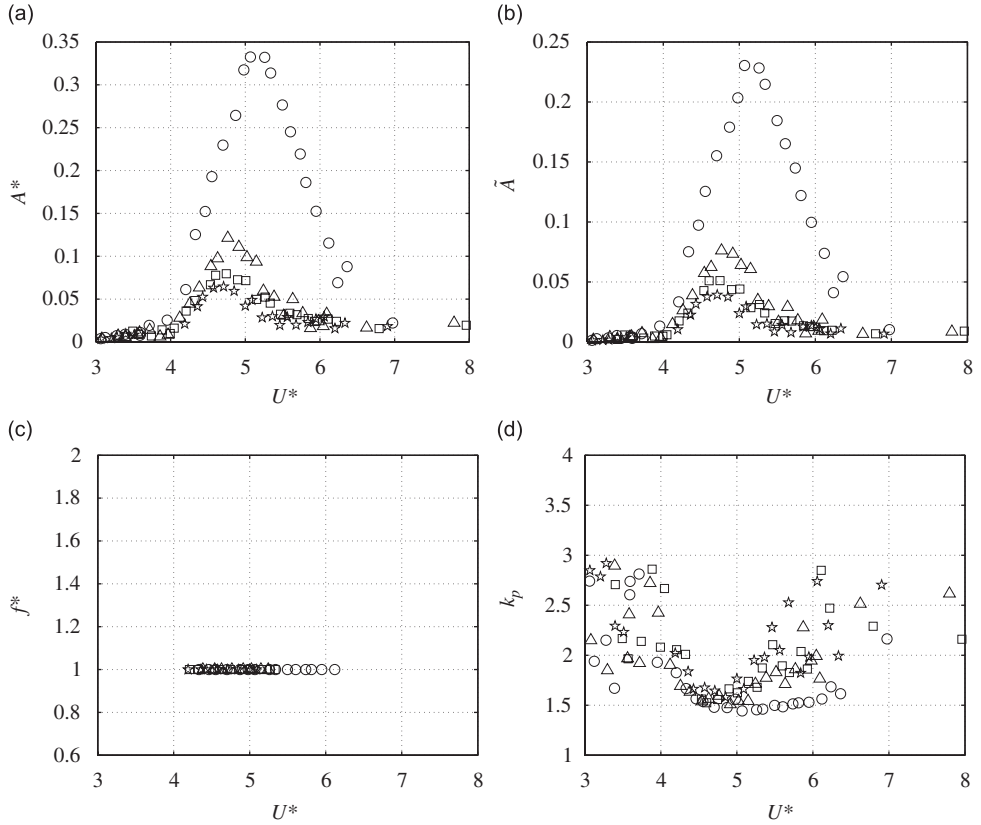

Fig. 6. Variation with U^* of the dimensionless amplitude, (a) A^*, of the standard deviation of the dimensionless amplitude, (b) $\widetilde{A}$, of the frequency ratio, (c) f^*, and of the peak factor, (d) k_p: ○, Run c_1; △, Run c_2; □, Run c_3; ☆, Run c_4.

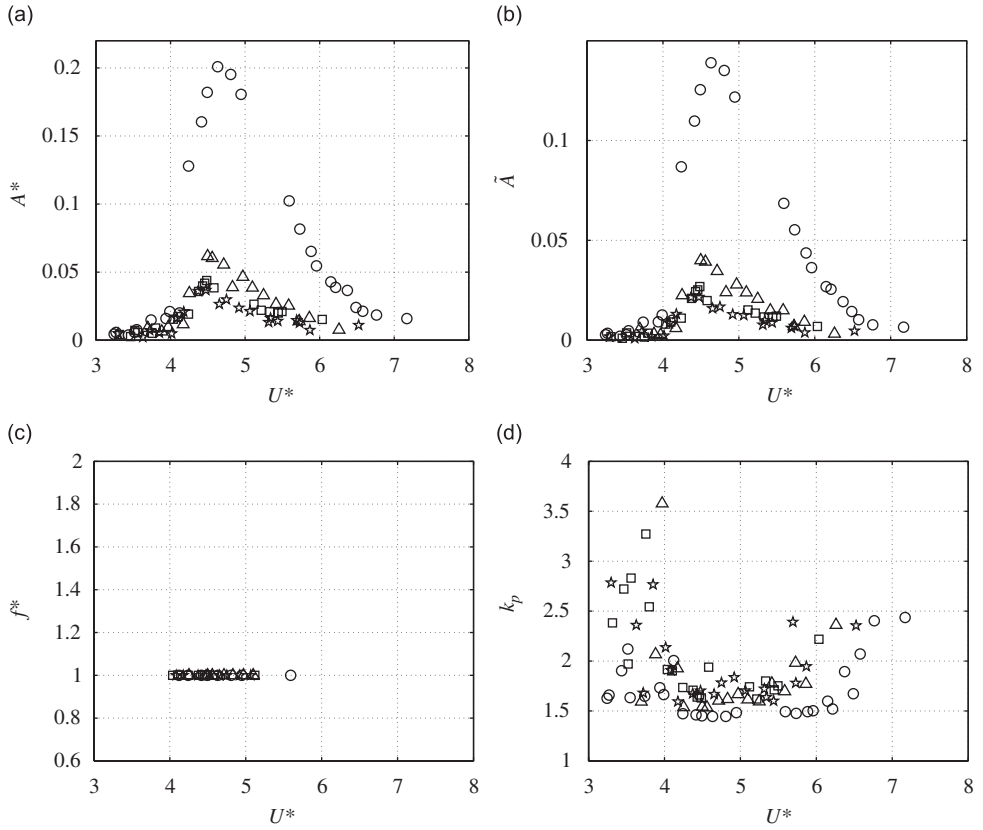

Fig. 7. Variation with U^* of the dimensionless amplitude, (a) A^*, of the standard deviation of the dimensionless amplitude, (b) $\widetilde{A}$, of the frequency ratio, (c) f^*, and of the peak factor, (d) k_p. ○, Run d_1; △, Run d_2; □, Run d_3; ☆, Run d_4.

4.1. Discussion of results

The response of a damped system undergoing synchronized oscillations depends upon whether the mass-damping parameter, $m^*\zeta$, is relatively small or large [see e.g. Khalak and Williamson, 1999], and upon Re [see e.g. Klamo et al., 2006]. The combinations of $m^*\zeta$ and Re may provide responses organized in two branches (initial and lower) or three branches (initial, upper and lower) as reported by Klamo et al. (2006).

In the present work, where relatively high levels of $m^*\zeta$ have been accounted for, various features have been observed varying Re_{eff} regimes and damping levels.

In laminar flow (Figs. 4(a) and (b)), as long as the mean flow velocity is increased, the quasi-steady amplitude of oscillation increases until it approaches its maximum value, then it drops and continues to decrease until the synchronization ends. This behaviour might justify the existence of the initial branch and the lower branch. The latter scales down when $m^*\zeta$ is increased as shown recently by Klamo et al. (2006).

The same behaviour may be ascertained for the smooth cylinder tested in low turbulence flow (Figs. 5(a) and (b)).

Different behaviours take place for both smooth and rough cylinders immersed in the high turbulence flow. In the case in which the smooth cylinder is considered, the response curve does not present any jump after the maximum value is approached (Figs. 6(a) and (b)). In presence of the rough cylinder, the response curves are more scattered (Figs. 7(a) and (b)). Such scattering may be attributed to the higher values of Re_{eff}.

It is interesting to linger over the existence of vortex shedding even crossing the *critical* Re_{eff} regime (see Table 3) which is characterized by the disappearance of this phenomenon for steady cylinders. If vortices may shed from the cylinder in the critical Re_{eff} regime, it is clear that the cylinder oscillations take the control of the vortex shedding and the synchronization may occur.

In laminar and low turbulence flows, after the synchronization end the vortex shedding frequencies depart from the Strouhal frequencies obtained by the steady cylinder tests (see Figs. 4(c) and 5(c)). It seems that St increases. Only the

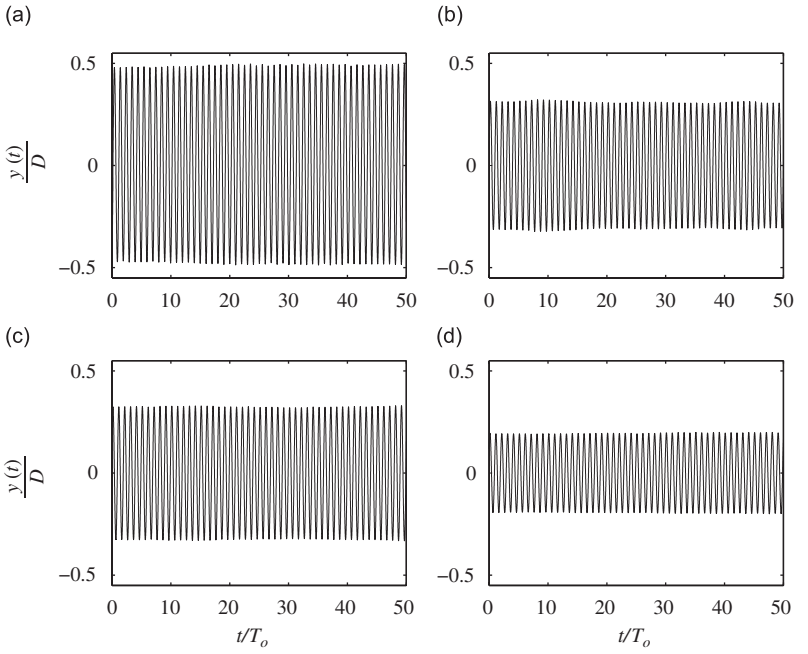

Fig. 8. Time histories of the dimensionless response, $y(t)/D$, at A^*_{max}, during the first 50 cycles: (a) Run a_1, $1/f_o = 0.220\,s$, $U^* = 5.83$; (b) Run b_1, $1/f_o = 0.220\,s$, $U^* = 5.77$; (c) Run c_1, $1/f_o = 0.220\,s$, $U^* = 5.07$ and (d) Run d_1, $1/f_o = 0.236\,s$, $U^* = 4.63$.

data of the lower damping configurations approach the respective Strouhal frequencies after the vortex capture vanishes.

In high turbulence flow, it is interesting to note that it has been possible to draw out f^* (Figs. 6(c) and 7(c)) only during the lock-in range. This is due to the fact that the operating Re_{eff} regime is the critical one, so it has not been possible to observe a distinct peak in the vortex wake spectra outside the lock-in range, since vortex shedding disappears in this regime.

In laminar and low turbulence flows, the maximum amplitude of oscillation attained by the cylinder manifests itself in the second half of the synchronization interval, and it is shifted towards its upper (right) bound (Figs. 4 and 5). In these flow conditions, the higher is the damping level the higher is the agreement of the highest amplitude of oscillation and the synchronization end. At higher Re_{eff}, the maximum response coincides with almost the centre of the lock-in range (Figs. 6 and 7).

During the synchronization regime, the peak factor tends gradually to the theoretical value $k_p = \sqrt{2}$ of a harmonic process (Figs. 4(d), 5(d), 6(d), and 7(d)), reaching the best accordance with that value when the maximum amplitude of oscillation is approached, coherently with the lower modulation, in amplitude and frequency, of the maximum limit cycle. Outside the lock-in, the peak factor approaches the typical values of random processes, theoretically in the range between 3.5 and 4.

Some time histories of the dimensionless amplitude of oscillation attained by the cylinder are shown in Fig. 8 where the effect of Re_{eff} on the response is clear: increasing Re_{eff} the response decreases.

The absolute maximum response, A^*_{max}, of each configuration decreases as a function of Sc (Fig. 9(a)): the higher is the damping level the lower is the maximum response attained by the cylinder in all the tested configurations. By fixing the damping level ζ, A^*_{max} decreases by increasing Re_{eff} (Fig. 9(b)). Moreover, in laminar flow (see Fig. 9(c)), when the damping level is increased, the maximum response, A^*_{max}, takes place at lower reduced velocities. This trend is emphasized when the turbulence level and the cylinder roughness increase and so whenever Re_{eff} increases (Fig. 9(c)).

In laminar and low turbulence flows (see Fig. 10), the synchronization range narrows when damping is increased. In particular, its lower bound draws back much less than the upper one which shows itself sensibly different passing through the lowest to the highest damping level. The range of synchronization exhibits some differences for both the smooth and the rough cylinders immersed in the flow with high turbulence (see Fig. 10): it broadens as long as the lowest damping is considered, whereas it narrows in the higher damping configurations. Nevertheless, in the latter cases,

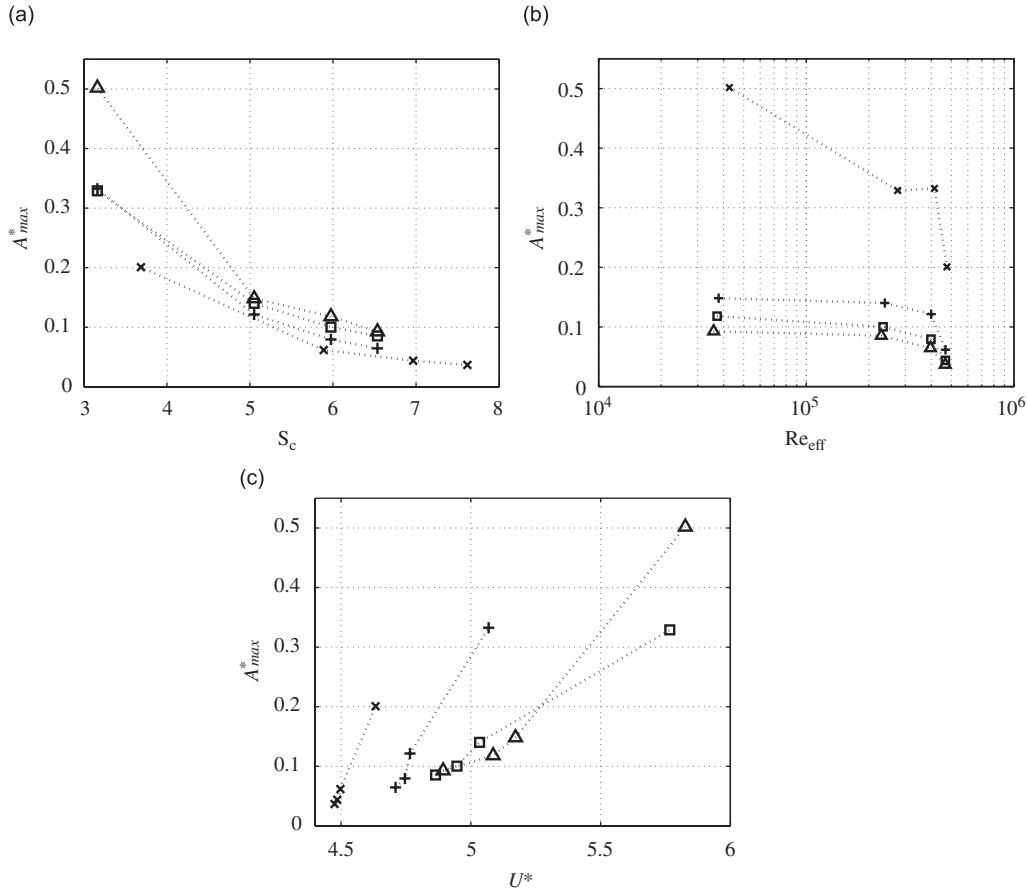

Fig. 9. (a) Variation of the maximum dimensionless amplitude, A^*_{max}, with the Scruton number, $Sc = \pi^2(m^*\zeta)$. △, Runs $a_1 - a_4$; □, Runs $b_1 - b_4$; +, Runs $c_1 - c_4$; ×, Runs $d_1 - d_4$. (b) Variation of the maximum dimensionless amplitude, A^*_{max} with the effective Reynolds number, Re_{eff}: $(\times, \zeta) = 0.0024$ (Runs a_1, b_1, c_1 and d_1); $(+, \zeta) = 0.0039$ (Runs a_2, b_2, c_2 and d_2); $(\square, \zeta) = 0.0046$ (Runs a_3, b_3, c_3 and d_3); $(\triangle, \zeta) = 0.0050$ (Runs a_4, b_4, c_4 and d_4). (c) Variation of the maximum dimensionless amplitude A^*_{max} with the reduced velocity, U^*: △, Runs $a_1 - a_4$; □, Runs $b_1 - b_4$; +, Runs $c_1 - c_4$; ×, Runs $d_1 - d_4$.

the wideness of the lock-in range does not narrow down prominently, on the contrary it remains almost constant and draws back slightly.

The relationship between the amplitude of oscillation and the wake correlation length, L_C, is more evident in laminar and low turbulence flows (Fig. 11(a)): the higher is the response amplitude the higher is L_C. In particular, in laminar flow, in the case of the smallest value of $m^*\zeta$, the cylinder oscillates highly, and the wake is almost fully correlated. In the presence of the high turbulence (see Fig. 11(a)), for both smooth and rough cylinders, the relationship between the amplitude of oscillation and the correlation of the vortex structure is no longer so marked since the correlation length decreases sensibly. It might be attributed to the fact that the wake becomes more three-dimensional. By keeping the damping level ζ constant, it is clear from Fig. 11(b) that the wake correlation length decreases with higher Re (or Re_{eff}).

Some questions may arise in analyzing the phase between the lift force and the synchronized oscillations of the cylinder. Models more and more refined may be considered. Here, with the aim of obtaining simple estimates, just the model proposed by Bearman (1965) has been considered. In this case, the equation of motion reads:

$$m\ddot{y} + c\dot{y} + ky = \tfrac{1}{2}C_y\rho_f DLU^2, \tag{5}$$

where m is the mass of the cylinder, c the linear material damping coefficient, k the linear spring constant, ρ_f is the fluid density, D and L are the diameter and the length of the cylinder, respectively, U is the steady flow velocity, and $C_y = F_L(t)/\frac{1}{2}\rho_f DU^2$ is the lift coefficient.

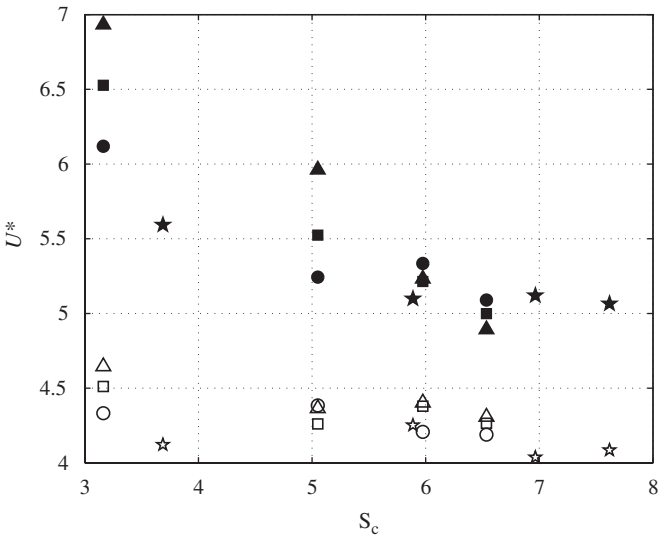

Fig. 10. Variation of the wideness of the lock-in range: the starting (open mark) and final (filled mark) reduced velocities, U^*, at lock-in are plotted versus the Scruton number, $Sc = \pi^2(m^*\zeta)$: ($\triangle, \blacktriangle$) laminar flow (Runs $a_1 - a_4$); ($\square, \blacksquare$) low turbulence flow (Runs $b_1 - b_4$); ($\circ, \bullet, \zeta$) high turbulence flow (Runs $c_1 - c_4$); ($\star, \bigstar$) high turbulence flow, rough cylinder (Runs $d_1 - d_4$).

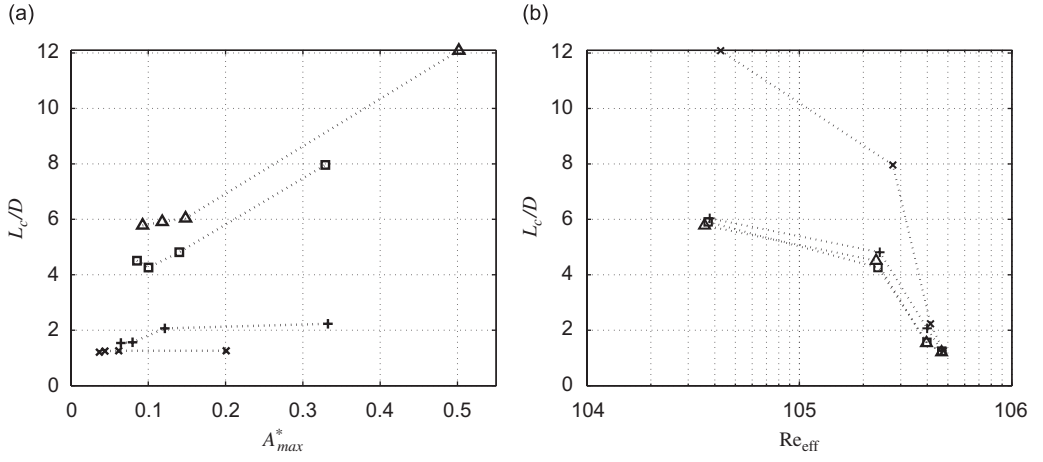

Fig. 11. (a) Variation of the correlation length, L_c/D, with the maximum dimensionless amplitude of oscillation, $A^*_{\max}$: $\triangle$, Runs $a_1 - a_4$; $\square$, Runs $b_1 - b_4$; $+$, Runs $c_1 - c_4$; $\times$, Runs $d_1 - d_4$. (b) Variation of the correlation length L_c/D with the effective Reynolds number, Re_{eff}: ($\times, \zeta$) = 0.0024 (Runs a_1, b_1, c_1 and d_1); ($+, \zeta$) = 0.0039 (Runs a_2, b_2, c_2 and d_2); ($\square, \zeta$) = 0.0046 (Runs a_3, b_3, c_3 and d_3); ($\triangle, \zeta$) = 0.0050 (Runs a_4, b_4, c_4 and d_4).

It is clear from Eq. (5) that the model describes a simple visco-elastic oscillator subjected to a fluid force provided by the surrounding flow. At lock-in the steady-state cylinder displacement and C_y are usually expressed in terms of a harmonic function. Therefore, since the wake and the cylinder have a common frequency of oscillation, f_{vs}, Eq. (5) may be solved for

$$C_y = C_L^* \sin(2\pi f_{vs} t + \varphi) \tag{6}$$

and

$$y = \hat{y} \sin(2\pi f_{vs} t), \tag{7}$$

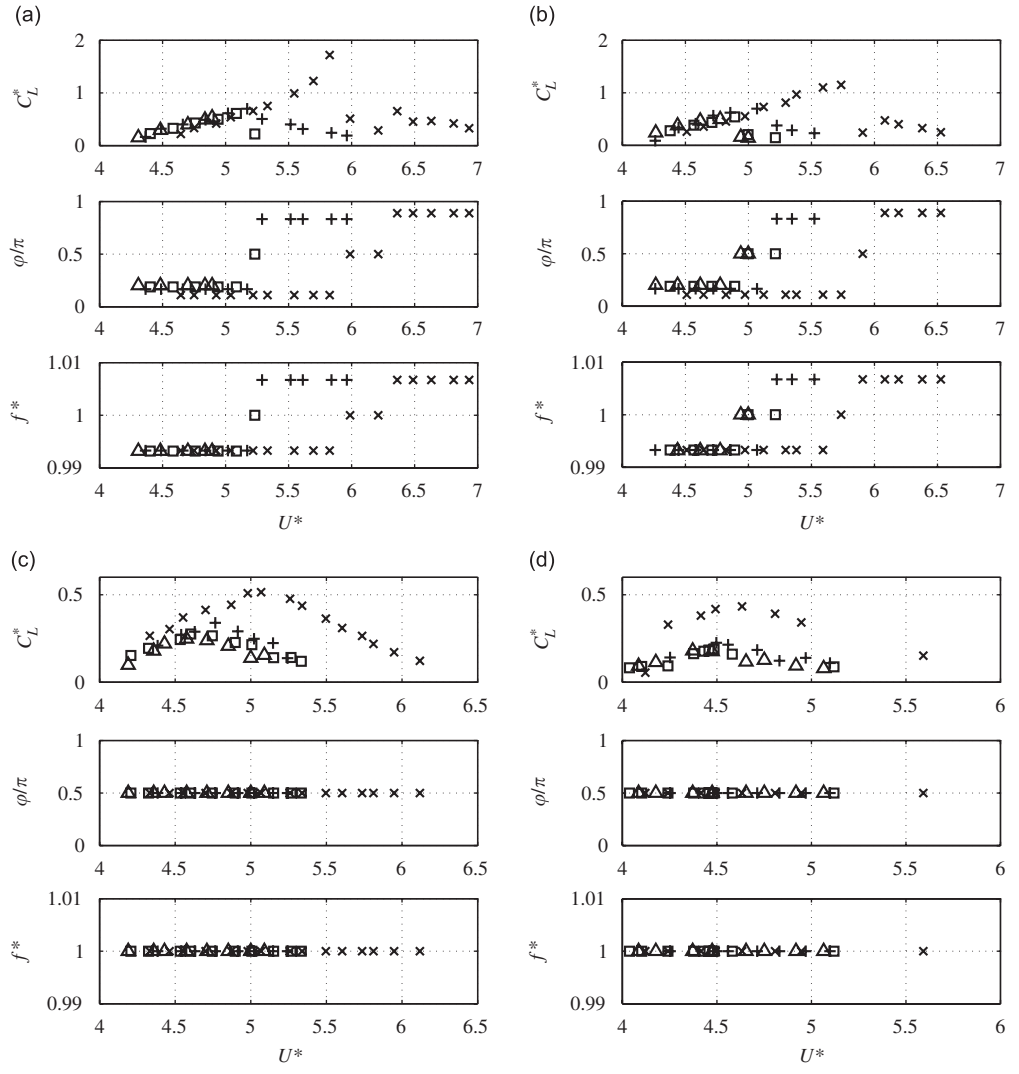

Fig. 12. Variation of the lift coefficient, C_L^*, of the phase between the lift and the cylinder motion, φ, and of the frequency ratio, f^*, along the lock-in range. (a) ×, Run a_1; +, Run a_2; □, Run a_3; △, Run a_4; (b) ×, Run b_1; +, Run b_2; □, Run b_3; △, Run b_4; (c) ×, Run c_1; +, Run c_2; □, Run c_3; △, Run c_4; (d) ×, Run d_1; +, Run d_2; □, Run d_3; △, Run d_4.

where $\hat{y}$ is the maximum value of the response time series obtained during the experimental tests, and C_L^* is the amplitude of the exciting force. In particular, one gets

$$C_L^* \cos(\varphi) = (1 - f^{*2}) 2\pi^3 m^* A^* U^{*-2} \tag{8}$$

and

$$C_L^* \sin(\varphi) = f^* 4\pi^3 m^* \zeta A^* U^{*-2}, \tag{9}$$

so that C_L^* may be computed by means of the following formula:

$$C_L^* = \sqrt{[C_L^* \cos(\varphi)]^2 + [C_L^* \sin(\varphi)]^2}. \tag{10}$$

The phase angle between the lift force and the cylinder displacement is given by the following well-known expression:

$$\varphi = \arctan\left(\frac{2\zeta f^*}{1 - f^{*2}}\right). \tag{11}$$

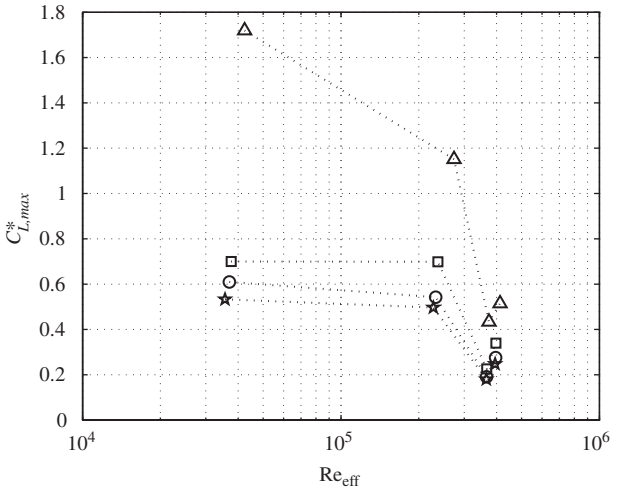

Fig. 13. Variation of maximum lift coefficient, $C^*_{L,\max}$, with the effective Reynolds number, Re_{eff}: $(\times,\zeta) = 0.0024$ (Runs a_1, b_1, c_1 and d_1); $(+,\zeta) = 0.0039$ (Runs a_2, b_2, c_2 and d_2); $(\square,\zeta) = 0.0046$ (Runs a_3, b_3, c_3 and d_3); $(\triangle,\zeta) = 0.0050$ (Runs a_4, b_4, c_4 and d_4).

Table 4
Comparison of the lift coefficient with the results of Feng (1968) and Fathi (2001) (the lift coefficient has been logged by means of pressure taps when the body was free to oscillate in air), and Carberry et al. (2001) (the lift coefficient has been logged by means of load cells when the cylinder was forced to oscillate in water with $A^*_{\max} = 0.5$, so $k_p = \sqrt{2}$)

	A^*	$\widetilde{A}$	$\tilde{C}_L$	$(\hat{C}_L)_{\max}$	Re
Feng (1968)	0.35	0.49	1.35	1.91	2.0×10^4
Fathi (2001)	0.42	0.59	1.31	1.85	4.5×10^4
Carberry et al. (2001)	0.35	0.5	1.34	1.90	2.3×10^3
Run a_1	0.34	0.48	1.17	1.72	4.3×10^4

The analysis above is based on the assumption that both the motion of the cylinder and the lift force are quasi-harmonic time series (see e.g. Fig. 8), since their spectra have narrow bandwidths. Nevertheless, frequency and amplitude of oscillations do not remain constant: they are more or less modulated during self-excited vibrations. So, the assumption of harmonic functions simplifies the problem but it avoids the issues concerning the real nature of the oscillations and forces.

The present analysis, however, would like to raise some questions regarding VIV at higher Re. Feng (1968) noted a jump in the response amplitude, simultaneous with a jump in φ. Zdravkovich (1982) showed that this phase jump was reflected by a switch in the timing of vortex shedding. In particular, Zdravkovich (1982) pointed out that two modes occurred in the lock-in range, and he also observed that the transition between them occurred crossing the maximum amplitude of oscillation. Ongoren and Rockwell (1988) observed this timing switch as f^* was increased through $f^* \approx 0.95$. Williamson and Roshko (1988) ascribed such phase jump to a change in the wake mode, from 2S (two vortices shed for each cycle of oscillation) to 2P (two pairs of vortices shed for each cycle of oscillation).

In laminar and low turbulence flows (see Fig. 12), a phase jump occurs for all the tested configurations, passing through the resonance ($f^* = 1$). Moreover, just before this phase shift, the responses approach their maximum value, $A^*_{\max}$ (see Figs. 4(a) and 5(a)). In high turbulence flow, both for smooth and rough cylinders, it is no longer possible to notice such phase shift since f^* is constantly unitary during the synchronization range.

Clearly, these results may be invalidated by the given assumptions of the very simple model adopted. Nevertheless, in laminar and low turbulence flows, some similarities exist with the results of Feng (1968), Zdravkovich (1982) and Ongoren and Rockwell (1988). So, the issue might concern the nature of the wake and its ability to change during lock-in at higher Re. Further work is required to delineate the vortex shedding mode before, during and after the transitional Re regime.

By considering the maximum value of the lift coefficient, $C^*_{L,\max}$, obtained by means of Eq. (10) within each experimental run, it is possible to plot its variation with Re as reported in Fig. 13. In Table 4, the value of $C^*_{L,\max}$ obtained in Run a_1 is tabulated together with those obtained by Feng (1968) and Fathi (2001) by means of pressure tap measurements on a freely vibrating circular cylinder in air, and by Carberry et al. (2001) by means of load cells used during forced oscillations of a circular cylinder immersed in water. The study of Table 4 highlights again that the response depends on both $m^*\zeta$ and Re: whenever the Reynolds numbers are close to each other, the lift coefficient depends on the amplitude of response and so on $m^*\zeta$ [see the results of Run a_1 and Fathi, 2001], whereas when the amplitudes of oscillation are close to each other [see the results of Run a_1, Feng, 1968; Carberry et al., 2001] the lift coefficient depends on Re. However, it should be remembered that the results obtained in the present work might be invalidated by the approximations of the simple model adopted. This suggests that direct measurements of the forces and more refined models are necessary to model such complex phenomena.

5. Conclusions

Experimental results of a freely vibrating cylinder in air have been discussed. The mass-damping parameter, $m^*\zeta$, is not the sole parameter influencing the response; the Reynolds number also plays an important role. If $m^*\zeta$ is fixed, the response drops as Re is increased. The present results confirm those obtained by Klamo et al. (2006), and by Govardhan and Williamson (2006) at lower Re. The oscillating cylinder takes control of the vortex shedding process in the critical Re_{eff} regime where, for a stationary cylinder, a sharp drop in the drag force is associated with a cessation of coherent vortex shedding. The effect of Re_{eff} is also evident by the study of the critical velocity, the wideness of the lock-in range, and the wake correlation length. Further studies may be necessary to assess the nature of the wake during lock-in, before and after the boundary layer transition Reynolds number. Another issue may concern the influence of both $m^*\zeta$ and higher Re on the well-known response hysteresis.

References

Achenbach, E., 1971. Influence of surface roughness on the cross-flow around a circular cylinder. Journal of Fluid Mechanics 46, 321.
Basset, A., 1888. On the motion of a sphere in a viscous liquid. Philosophical Transactions Royal Society of London 179, 43–68.
Basu, R., 1986. Aerodynamic forces on structures of circular cross sections. Part 2. The influence of turbulence and three-dimensional effects. Journal of Wind Engineering and Industrial Aerodynamics 24, 33–59.
Bearman, P., 1965. Investigation of the flow behind a two-dimensional model with a blunt trailing edge and fitted with splitter plates. Journal of Fluid Mechanics 21, 241.
Bishop, R., Hassan, A., 1964. The lift and drag forces on a circular cylinder in a flowing fluid. Proceedings of Royal Society of London Series A 277, 32–50, 51–75.
Blackburn, H., Melbourne, W., 1996. The effects of free stream turbulence on sectional lift forces on a circular cylinder. Journal of Fluid Mechanics 306, 267–292.
Blevins, R., 1990. Flow-Induced Vibration, second ed. Van Nostrand Reinhold, New York.
Buresti, G., Launaro, F., 1980. Pressure measurements around a circular cylinder in cross-flow near a plane surface. AIA Report 80-1, Atti dell'Istituto di Aeronautica, Università di Pisa, italy.
Buresti, G., Martini, M., 1980. Experimental research on the effects of surface roughness on the cross-flow around circular cylinders. AIA Report 80-2.
Carberry, J., Sheridan, J., Rockwell, D., 2001. Forces and wake modes of an oscillating cylinder. Journal of Fluids and Structures 15, 523–532.
ESDU, 1970. Fluid forces acting on circular cylinders for application in general engineering Item No. 70013.
ESDU, 1980. Mean forces, pressures and flow field velocities for circular cylindrical structures: single cylinder with two-dimensional flow Item No. 80025.
ESDU, 1996. Response of structures to vortex shedding: structures of circular or polygonal cross section Item No. 96030.
Fathi, S., 2001. Vibrazioni strutturali across-wind per distacco dei vortici. Ph.D. Thesis, University of Chieti-Pescara, Italy.
Feng, C., 1968. The measurement of vortex induced effects in flow past stationary and oscillating circular and d-section cylinders. Master Thesis, Department of Mechanical Engineering, The University of British Columbia, Canada.
Gerrard, J.H., 1966. The machanics of the formation region of vortices behind bluff bodies. Journal of Fluid Mechanics 25, 401–413.
Govardhan, R., Williamson, C., 2000. Modes of vortex formation and frequency response of a freely vibrating cylinder. Journal of Fluid Mechanics 420, 85–130.
Govardhan, R., Williamson, C., 2006. Defining the ''modified Griffin plot'' in vortex-induced vibration: revealing the effect of Reynolds number using controlled damping. Journal of Fluid Mechanics 561, 147–180.
Griffin, O., Ramberg, S., 1975. On the vortex strength and drag in bluff-body wakes. Journal of Fluid Mechanics 69, 721–728.

Humphries, J.A., Walker, D., 1988. Vortex-excited response of large-scale cylinders in sheared flow. ASME Journal of Offshore Mechanics and Arctic Engineering 110, 272–277.
Khalak, A., Williamson, C., 1999. Motions, forces and mode transitions in vortex-induced vibrations at low mass-damping. Journal of Fluids and Structures 13, 813–851.
Klamo, J., Leonard, A., Roshko, A., 2006. The effects of damping on the amplitude and frequency response of a freely vibrating cylinder in cross-flow. Journal of Fluids and Structures 22, 845–856.
Lienhard, J., 1966. Synopsis of lift, drag and vortex frequency data for rigid circular cylinder. Washington State University, College of Engineering, Research Division Bulletin 300.
Novak, M., Tanaka, H., 1975. Pressure correlations on a vibrating cylinder. In: Eaton, K.J. (Ed.), Fourth International Conference on Wind Effects on Buildings and Structures, vol. 1. Cambridge University Press, Cambridge, pp. 227–232.
Ongoren, A., Rockwell, D., 1988. Flow structure from an oscillating cylinder. Part 1. Mechanics of phase shift and recovery in the near wake. Journal of Fluid Mechanics 191, 197–223.
Pastò, S., 2005. Fatigue-induced risk assessment of slender structures with circular cross-section at lock-in. Doctoral Thesis, University of Florence, Italy, TU-Braunschweig, Germany.
Ramberg, S., Griffin, O., 1976. The effects of vortex coherence, spacing and circulation on the flow-induced forces on vibrating cables and bluff structures. Report 7945, Naval Research Laboratory, Washington, DC, USA.
Sarpkaya, T., 1977. Transverse oscillations of a circular cylinder in uniform flow. Part 1. Technical Report NPS-69SL77071, Naval Postgraduate School, Monterey, CA, USA.
Sarpkaya, T., 1978. Fluid forces on oscillating cylinders. Journal of Waterway Port Coastal and Ocean Division ASCE 104, 275–290.
Sarpkaya, T., 2000. Resistance in unsteady flow: search for an in-line force model. International Journal of Offshore and Polar Engineering 10, 249–254.
Sarpkaya, T., 2004. A critical review of the intrinsic nature of vortex-induced vibrations. Journal of Fluids and Structures 19, 389–447.
Schewe, G., 2001. Reynolds-number effects in flow around more-or-less bluff bodies. Journal of Wind Engineering and Industrial Aerodynamics 89, 1267–12892.
Scruton, C., Rogers, E., 1971. Steady and unsteady wind loading of buildings and structures. Philosophical Transactions of the Royal Society A 269, 353–383.
Singh, S., Mittal, S., 2005. Vortex-induced oscillations at low Reynolds numbers: Hysteresis and vortex-shedding modes. Journal of Fluids and Structures 20, 1085–1104.
Skop, R., 1974. On modelling vortex-excited oscillations. NRL Memo. Report 2927.
Surry, D., 1969. The effect of high turbulence intensity on the aerodynamics of a rigid circular cylinder at subcritical Reynolds numbers. UTIAS Report No. 142.
Tanida, Y., Okajima, A., Watanabe, Y., 1973. Stability of a circular cylinder oscillating in uniform flow or wake. Journal of Fluid Mechanics 61, 769–784.
Toebes, G., 1969. The unsteady flow and wake near an oscillating cylinder. ASME Journal of Basic Engineering 91, 493–502.
Vickery, B., 1990. Progress and problems in the prediction of the response of prototype structures to vortex-induced vibration. Journal of Wind Engineering and Industrial Aerodynamics 33, 181–196.
von Karman, T., 1948. Progress in the statistical theory of turbulence. Journal of Maritime Research 7.
Williamson, C., 1996. Vortex dynamics in the cylinder wake. Annual Review of Fluid Mechanics 28, 477–539.
Williamson, C., Govardhan, R., 2004. Vortex-induced vibrations. Annual Review of Fluid Mechanics 36, 413–455.
Williamson, C., Roshko, A., 1988. Vortex formation in the wake of an oscillating cylinder. Journal of Fluids and Structures 2, 355–381.
Zdravkovich, M., 1982. Modification of vortex shedding in the synchronization range. ASME Journal of Fluids Engineering 104, 513–517.
Zdravkovich, M.M., 1997. Flow Around Circular Cylinders: Vol. 1. Fundamentals. Oxford University Press, Oxford, England.